Official citation: Hellmer, H. H., Kauker, F., Timmermann, R., Determann, J. & Rae, J. Twenty-first-century warming of a large Antarctic ice-shelf cavity by a redirected coastal current, *Nature* **485 (7397),** 225-228 (2012). doi: 10.1038/nature11064 (Postprint: http://hdl.handle.net/10013/epic.39299.d001)

21^{st}-century warming of a large Antarctic ice shelf cavity by a redirected coastal current

Hartmut H. Hellmer*, Frank Kauker*, Ralph Timmermann*, Jürgen Determann* & Jamie Rae†

*Alfred Wegener Institute for Polar and Marine Research, D-27570 Bremerhaven, Germany

†Met Office Hadley Centre, Exeter, EX1 3PB, United Kingdom

The Antarctic ice sheet loses mass at its fringes bordering the Southern Ocean marginal seas. At this boundary, warm circumpolar water can override the continental slope front, reaching the grounding line[1,2] via submarine glacial troughs and causing high rates of melting at deep ice shelf bases[3,4]. The interplay between ocean currents and continental bathymetry is therefore likely to influence future rates of mass loss. Here we show that a redirection of the coastal current into the Filchner Trough and underneath the Filchner-Ronne Ice Shelf during the second half of the 21^{st} century leads to increased movement of warm waters into the deep southern subsurface ice cavity. Water temperatures in the cavity increase by more than 2 °C and boost average basal melting from 0.2 m yr^{-1} (82 Gt yr^{-1}) to almost 4 m yr^{-1} (1600 Gt yr^{-1}). Our results, based on the output of a coupled ice-ocean model forced by a range of atmospheric outputs from

the HadCM3[5] climate model, suggest that the changes are primarily due to an increase of ocean-surface stress in the southeastern Weddell Sea due to disintegration of the formerly consolidated sea ice cover. The projected ice loss at the Filchner-Ronne Ice Shelf base represents 80% of the present Antarctic surface mass balance[6]. Thus, the quantification of basal mass loss under changing climate conditions is of paramount importance for projections regarding the dynamics of Antarctic ice streams and ice shelves, and global sea level rise.

The Weddell Sea (Fig. 1) is dominated by a cyclonic gyre circulation which allows Circumpolar Deep Water to enter only from the east[7]. Within the southern branch of the gyre the water mass can be identified as the Weddell Sea's temperature maximum at a depth of ~300 m. The temperature decreases from 0.9 °C at the Greenwich Meridian[7] to 0.6 °C off the tip of the Antarctic Peninsula[8]. Only traces of the relatively warm water penetrate onto the broad southern continental shelf[9], reaching the Filchner Ice Shelf front with temperatures of -1.5 °C[10]. However, no indications exist that this water mass advances far into the ice shelf cavity[11]. Instead, locally formed High Salinity Shelf Water with temperatures at the surface freezing point (~ -1.89 °C) fuels a sub-ice shelf circulation which brings the heat to the deep southern grounding line. High Salinity Shelf Water is the densest water mass in the Weddell Sea, formed by brine rejection during sea ice formation on a southward sloping continental shelf. The need for a dense water mass to transport heat to the grounding line was used as an argument for the Filchner-Ronne Ice Shelf to be protected in a warmer climate[12]. This hypothesis assumes that rising atmospheric temperatures reduce sea ice formation and thus the densification of the shelf water masses. However, this view considers solely the formation of dense continental shelf water masses in a warmer climate, though a less consolidated sea ice cover might also influence the Weddell Sea circulation including the course of the coastal current.

The marine based West Antarctic Ice Sheet (WAIS) has the potential to contribute 3.3 m to the global, eustatic sea level rise[13]. Its ice shelves fringing the Amundsen Sea are exposed today to Circumpolar Deep Water with temperatures above 1 °C. This water mass cascades nearly undiluted from the continental shelf break into ∼1000-m deep trenches underlying the floating extensions of ice streams which drain the WAIS[14]. Some WAIS ice streams also feed the 449 000 km^2 Filchner-Ronne Ice Shelf (Fig. 1), forming the southern coast of the Weddell Sea. These ice streams pass over mountain ranges and thus would not face an increase in basal melting as the grounding line retreats. However, major ice streams entering the Filchner-Ronne Ice Shelf discharge large catchment basins of the East Antarctic Ice Sheet[15]. Once afloat this ice interacts with the waters of the Weddell Sea.

We forced the Bremerhaven Regional Ice-Ocean Simulations (BRIOS) model[16] with the atmospheric output of two versions of the HadCM3 climate model (Tab. 1). While HadCM3-A is the baseline simulation used in perturbed physics ensembles[17], HadCM3-B is a model configuration with an interactive carbon cycle and vegetation employed in the ENSEMBLES project[18]. We used the output of both 20th- century simulations (HadCM3-A: 1900–1999, HadCM3-B: 1860–1999) and the climate change scenarios E1[19] (2000–2199) and A1B[20] (2000–2099/2199) (Tab. 1). E1 and A1B are characterized by different CO_2 emission scenarios with atmospheric concentrations reaching 450 ppmV and 700 ppmV by the year 2100, respectively. BRIOS is a coupled ice-ocean model which resolves the Southern Ocean south of 50° S zonally at 1.5° and meridionally at $1.5° \times \cos\phi$. The water column is variably divided into 24 terrain-following layers. The sea-ice component is a dynamic-thermodynamic snow/ice model with heat budgets for the upper and lower surface layers[21] and a viscous-plastic rheology[22]. BRIOS considers the ocean-ice shelf interaction underneath ten Antarctic ice shelves[16,23] with time-invariant thicknesses, assuming flux divergence and mass balance to be in dynamical equilibrium. The model has been successfully validated by the comparison with mooring and buoy observations regarding, e.g., Weddell gyre transport[16], sea ice thickness distribution and drift in Weddell and Amundsen seas[24,25], and sea ice concentration related to iceberg drift[26].

Ocean characteristics of the simulations forced with 20^{th}- century output of both HadCM3-A/B agree well with those from hindcasts using the NCEP-reanalysis[27]. In the following, we focus on the results of the runs forced with the output from HadCM3-B for the A1B scenario, because the A1B-scenario provides stronger signals and only the HadCM3-B simulations cover a 200-year period until the end of the 22^{nd} century. For the simulated present-day period, a slope front separates shelf water at the surface freezing point from relatively warm water, advected to the southern Weddell Sea by the coastal current. However, starting around 2036 pulses of warm water cross sporadically the 700-m deep sill of the Filchner Trough at its eastern flank (Fig. 1) but do not reach the ice shelf front (e.g. Fig. 2: 2037). As early as 2070 water warmer than 0 °C begins to enter continously the Filchner Trough (Fig. 2: 2075) reaching the grounding lines of the southern tributaries six years later (Fig. 2: 2081). After an additional 14 years the whole trough plus the southern half of the Ronne cavity are filled with water of open ocean origin (Fig. 2: 2095). This corresponds to a warming of the deep southern cavity by more than 2 °C. The sporadic flow of warm water into the Filchner Trough during the 21^{st} century as well as its southward propagation is also suggested by results of the finite element model FESOM[28] when forced with the HadCM3-B_A1B output (see Supplementary Information). FESOM is a coupled ice-ocean model of different model architecture with an eddy-permitting resolution. Therefore, the model is expected to react more intensely to moderate perturbations in atmosphere and sea ice. Due to the higher resolution of the marginal seas ($\sim$10 km) in FESOM, the warm water pulses reach the interior of the Filchner Ice Shelf cavity less diluted (Fig. S4) and thus cause earlier significant increases in basal mass loss (Fig. S5).

The analysis of the forcing fields and the BRIOS output reveals that the redirection of the coastal current in the southeastern Weddell Sea is caused locally by an interplay between several climate components. During the 21^{st} century a continuous atmospheric surface warming (up to 4 °C per century) decreases the sensible heat loss of the ocean. Together with an increase in downward long-wave radiation (up to 10 W m^{-2} per century) this reduces thickness and concentration of the sea ice, allowing an enhancement of its drift speed and thus a more efficient momentum transfer to the ocean surface off Luitpold Coast (Fig. 3a,b). The enhanced surface stress, not related to an increase in atmospheric wind stress, directs the coastal current southward towards the Filchner Ice Shelf front, as it approaches the 700-m deep sill of the Filchner Trough. The importance of the different atmospheric forcing variables for the redirection of the coastal current and thus the increase in melting at the Filchner-Ronne Ice Shelf base is investigated by means of additional sensitivity experiments, outlined in the Supplementary Information. Since about 80% of the changes occur in the 21^{st} century, these experiments are confined to the period 2000–2099. The first simulation applies detrended atmospheric forcing variables only followed by runs in which the trends of 2-m temperature or/and long-wave downward radiation were consecutively added.

The warming of the whole Filchner-Ronne Ice Shelf cavity by more than 2 °C boosts average basal melting from 0.2 m yr^{-1} to 4 m yr^{-1} at the end of the 21^{st} century with the maximum exceeding 50 m yr^{-1} near the deep southern grounding line. The values correspond to a jump of the basal mass loss from 82 Gt yr^{-1} to roughly 1600 Gt yr^{-1} (Fig. 3c), representing 64% of the simulated circumpolar Antarctic total. The latter increases within two decades from $\sim$1000 Gt yr^{-1} to roughly 2500 Gt yr^{-1}. In contrast, basal mass loss beneath the Ross Ice Shelf remains constant at $\sim$80 Gt yr^{-1}. A similar drastic change in Filchner-Ronne and circumpolar basal mass loss, though with delays of 10 years and 50 years, also happens for the simulations (Tab. 1) forced with the A1B-output of HadCM3-A and the E1-output of HadCM3-B (Fig. 3c), respectively.

Due to the assumption of fixed ice shelf thicknesses, we cannot accurately predict basal mass losses for long periods of high melting. However, if we assume grounding lines to retreat into deeper basins[29], our melt rates have to be considered as lower bounds. In addition, numerical experiments show that ice shelves adjust to perturbations in ocean temperature on timescales ranging from several decades to a few centuries[30].

As a consequence of the increased freshwater input due to ice shelf basal melting, the Weddell Sea surface layer and the water masses on the whole southern and western continental shelves freshen rapidly. Today the high salinity shelf water of these areas is one ingredient for the formation of deep and bottom waters of the Weddell Sea[7,31]. These water masses change their characteristics as the shelf water freshens.

Given the spread among the climate scenarios and the different model realisations, we do not intend to predict the exact date of the changes in the circulation of the southern Weddell Sea. Instead, we emphasize the sensitivity of a small Antarctic coastal region to climate change with potentially severe consequences for the mass balance of a large Antarctic ice shelf. The extent to which this influences the dynamics of the East Antarctic Ice Sheet is subject to further experiments, forcing a coupled ice sheet/shelf model with the predicted temperature perturbation. The use of the output of two different configurations of HadCM3 for different scenarios and the confirmation of the BRIOS results by FESOM, a coupled ice-ocean model with higher resolution and different model architecture, narrows down unavoidable uncertainties when dealing with climate change related processes. Therefore, we are confident that our proposed mechanism is not a model artefact but a close-to-reality mechanism. Consequently, we welcome the effort to monitor the coastal current during the upcoming expeditions to the southeastern Weddel Sea.

References

1. Walker, D. P., et al. Oceanic heat transport onto the Amundsen Sea shelf through a submarine glacial trough. *Geophys. Res. Lett.* **34,** doi:10.1029/2006GL028154 (2007).

2. Hellmer, H. H., Jacobs, S. S. & Jenkins, A. Oceanic erosion of a floating Antarctic glacier in the Amundsen Sea. *Ocean, Ice, and Atmosphere: Interactions at the Antarctic Continental Margin*, (eds Jacobs, S. S. & Weiss, R. F.) **75,** 83-99 (AGU, Washington, D.C., 1998).

3. Jacobs, S. S., Jenkins, A., Giulivi, C. & Dutrieux, P. Stronger ocean circulation and increased melting under Pine Island Glacier ice shelf. *Nature Geoscience* doi:10.1038/ngeo1188 (2011).

4. Payne, A. J., Holland, P. R., Shepherd, A. P., Rutt, I. C., Jenkins, A. & Joughin, I. Numerical modeling of ocean-ice interactions under Pine Island Bay's ice shelf. *J. Geophys. Res.* **112,** doi:10.1029/2006JC003733 (2007).

5. Gordon, C., et al. The simulation of SST, sea ice extents and ocean heat transports in a version of the Hadley Centre coupled model without flux adjustments. *Clim. Dyn.* **16,** 147–168 (2000).

6. Rignot, E. et al. Acceleration of the contribution of the Greenland and Antarctic ice sheets to sea level. *Geophys. Res. Lett.* **38,** doi:10.1029/2011GL046583 (2011).

7. Schröder, M. & Fahrbach, E. On the structure and the transport in the eastern Weddell Gyre. *Deep-Sea Res. Part II* **46,** 501-527 (1999).

8. Schröder, M., Hellmer. H. H. & Absy, J. M. On the near-bottom variability at the tip of the Antarctic Peninsula. *Deep-Sea Res. Part II* **49,** 4767-4790 (2002).

9. Nicholls, K. W., Boehme, L., Biuw, M. & Fedak, M. A. Wintertime ocean conditions over the southern Weddell Sea continental shelf, Antarctica. *Geophys. Res. Lett.* **35,** doi:10.1029/2008GL035742 (2008).

10. Foldvik, A., Gammelsrød, T. & Tørresen T. Circulation and water masses on the southern Weddell Sea shelf. *Oceanology of the Antarctic Continental Shelf*, (ed Jacobs, S. S.) **43,** 5-20 (AGU, Washington, D.C., 1985).

11. Makinson, K. & Nicholls, K. W. Modeling tidal currents beneath Filchner-Ronne Ice Shelf and the adjacent continental shelf: Their effect on mixing and transport. *J. Geophys. Res.* **104,** 13449-13465 (1999).

12. Nicholls, K. W. Predicted reduction in basal melt rates of an Antarctic ice shelf in a warmer climate. *Nature* **388,** 460–462 (1997).

13. Bamber, J. L., Riva, R. E. M., Vermeersen, B. L. A. & LeBrocq, A. Reassessment of the potential sea-level rise from a collapse of the West Antarctic Ice Sheet. *Science* **324,** 901–903 (2009).

14. Jenkins, A., et al. Observations beneath Pine Island Glacier in West Antarctica and implications for its retreat. *Nature Geoscience* **3,** 468–472 (2010).

15. Bamber, J. L., Vaughan, D. G. & Joughin, I. Widespread complex flow in the interior of the Antarctic ice sheet. *Science* **287,** 1248-1250 (2000).

16. Beckmann, A., Hellmer, H. H. & Timmermann, R. A numerical model of the Weddell Sea: Large-scale circulation and water mass distribution. *J. Geophys. Res.* **104,** 23375-23391 (1999).

17. Collins, M. et al. Climate model errors, feedbacks and forcings: a comparison of perturbed physics and multi-model ensembles. *Clim. Dyn.* **36,** doi:10.1007/s00382-010-0808-0 (2011).

18. Johns, T. C., et al. Climate change under aggressive mitigation: The ENSEMBLES multi-model experiment. *Clim. Dyn.* doi:10.1007/s00382-011-1005-5 (2011).

19. Lowe, J. A., et al. New study for climate modelling, analyses, and scenarios. *EOS Trans AGU* **90,** 181–182 (2009).

20. Nakicevovic, N., et al. IPCC Special Report on Emissions Scenarios. *Cambridge University Press, Cambridge,UK* http://www.grida.no/publications/other/ipcc_sr/?src=/climate/ipcc/emission/ (2000).

21. Parkinson C. L. & Washington, W. M. A large-scale numerical model of sea ice. *J. Geophys. Res.* **84,** 311–337 (1979).

22. Hibler III, W. D. A dynamic-thermodynamic sea ice model. *J. Phys. Oceanogr.* **9,** 815-846 (1979).

23. Hellmer, H. H. Impact of Antarctic ice shelf melting on sea ice and deep ocean properties. *Geophys. Res. Lett.* **31,** doi:10.1029/2004GL019506 (2004).

24. Timmermann, R., Beckmann, A. & Hellmer, H. H. Simulations of ice-ocean dynamics in the Weddell Sea: 1. Model configuration and validation. *J. Geophys. Res.* **107,** doi:10.1029/2000JC000741 (2002).

25. Assmann, K. M., Hellmer, H. H. & Jacobs, S. S. Amundsen Sea ice production and transport. *J. Geophys. Res.* **110,** doi:10.1029/2004JC002797 (2005).

26. Lichey, C. & Hellmer, H. H. Modeling giant-iceberg drift under the influence of sea ice in the Weddell Sea, Antarctica. *J. Glaciol.* **47,** 452–460 (2001).

27. Kalnay, E. M., et al. The NCEP/NCAR 40-year reanalysis project. *Bull. Amer. Meteor. Soc.* **77,** 437–472 (1996).

28. Timmermann, R., et al. Ocean circulation and sea ice distribution in a finite element global sea ice–ocean model, *Ocean Modelling* **27,** doi:10.1016/j.ocemod.2008.10.009 (2009).

29. Timmermann, R., et al. A consistent dataset of Antarctic ice sheet topography, cavity geometry, and global bathymetry, *Earth Syst. Sci. Data* **2,** 261–273 doi:10.5194/essd-2-261-2010 (2010).

30. Walker, R. T. & Holland, D. M. A two-dimensional coupled model for ice shelf-ocean interaction. *Ocean Model* **17,** 123–139 (2007).

31. Gordon, A. L., Visbeck, M. & Huber, B. Export of Weddell Sea deep and bottom water. *J. Geophys. Res.* **106,** 9005–9017 (2001).

Acknowledgements

We thank C. Wübber for providing a stable computer performance at the Alfred-Wegener-Institute for Polar and Marine Research (AWI), the Ice2Sea community for helpful discussions during project meetings, and J. Ridley (MOHC), M. Martin (PIK), and A. Levermann (PIK) for critical comments on the manuscript. This work was supported by funding to the Ice2Sea programme from the European Union 7^{th} Framework Programme, grant number 226375. This is Ice2Sea contribution number 41.

Author contributions

H.H.H. had the idea to force BRIOS with IPCC-scenarios, did 50% of the BRIOS simulations, conducted a significant part of the analysis of model output, wrote the main text of the paper and participated in the figure preparation. F.K. did 50% of the BRIOS simulations, conducted the analysis of the atmospheric forcing, and wrote the 'Supplementary Information'. R.T. did all FESOM simulations, was involved in the analysis of model output and prepared most of the figures. J.D. provided the glaciological expertise for the interpretation of the model results related to basal mass loss. J.R. extracted the atmospheric forcings for all simulations and was involved in the analysis of model output. All authors participated in the discussion on model results and the draft of the paper.

Additional information

The authors declare no competing financial interests. Supplementary Information is linked to the online version of the paper at www.nature.com/nature. Reprints and permissions information is available online at http://www.nature.com/reprints. Correspondence and requests for materials should be addressed to H.H.H.

Table 1: List of BRIOS model experiments with the atmospheric output of the climate models HadCM3-A and HadCM3-B. HadCM3-A forcing only extends till 2099 and is not available for the E1 scenario. E1 and A1B are characterized by different CO_2 emission scenarios with atmospheric concentrations reaching 450 ppmV and 700 ppmV by the year 2100, respectively.

Model	Simulation	Period
HadCM3-A	20^{th}century	1900–1999
HadCM3-A	A1B	2000–2099
HadCM3-B	20^{th}century	1860-1999
HadCM3-B	A1B	2000–2199
HadCM3-B	E1	2000–2199

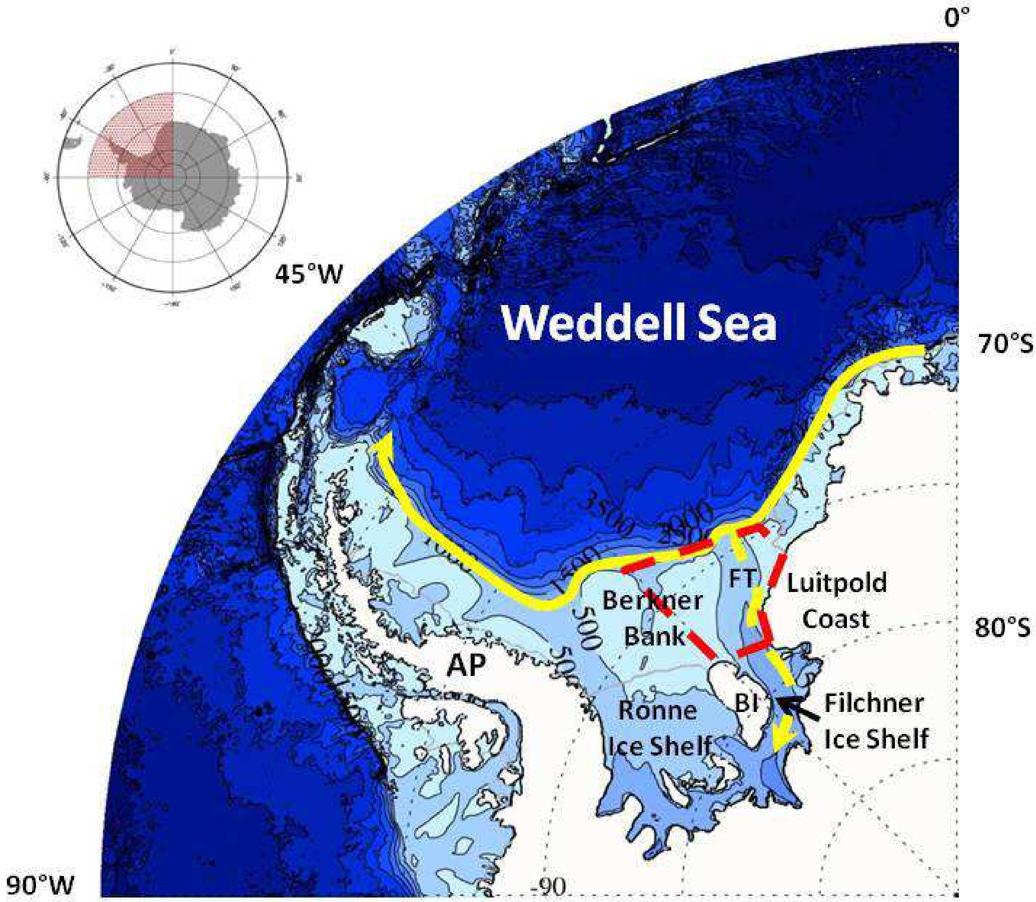

Figure 1: **Map of Weddell Sea bathymetry south of 60° S.** Bathymetry is based on RTopo-1[29] with colour contour interval 500 m. Inset shows location within the circumpolar Southern Ocean with red hatched area representing the model domain. Solid yellow arrow marks today's course of the coastal current in the Weddell Sea. The possibility of pulsing into the Filchner Trough (FT) is marked by the dashed yellow arrow. The region bounded by the dashed red line provided the integrated/mean values for Fig. 3. Solid gray line indicates the ice shelf fronts. AP = Antarctic Peninsula, BI = Berkner Island.

259

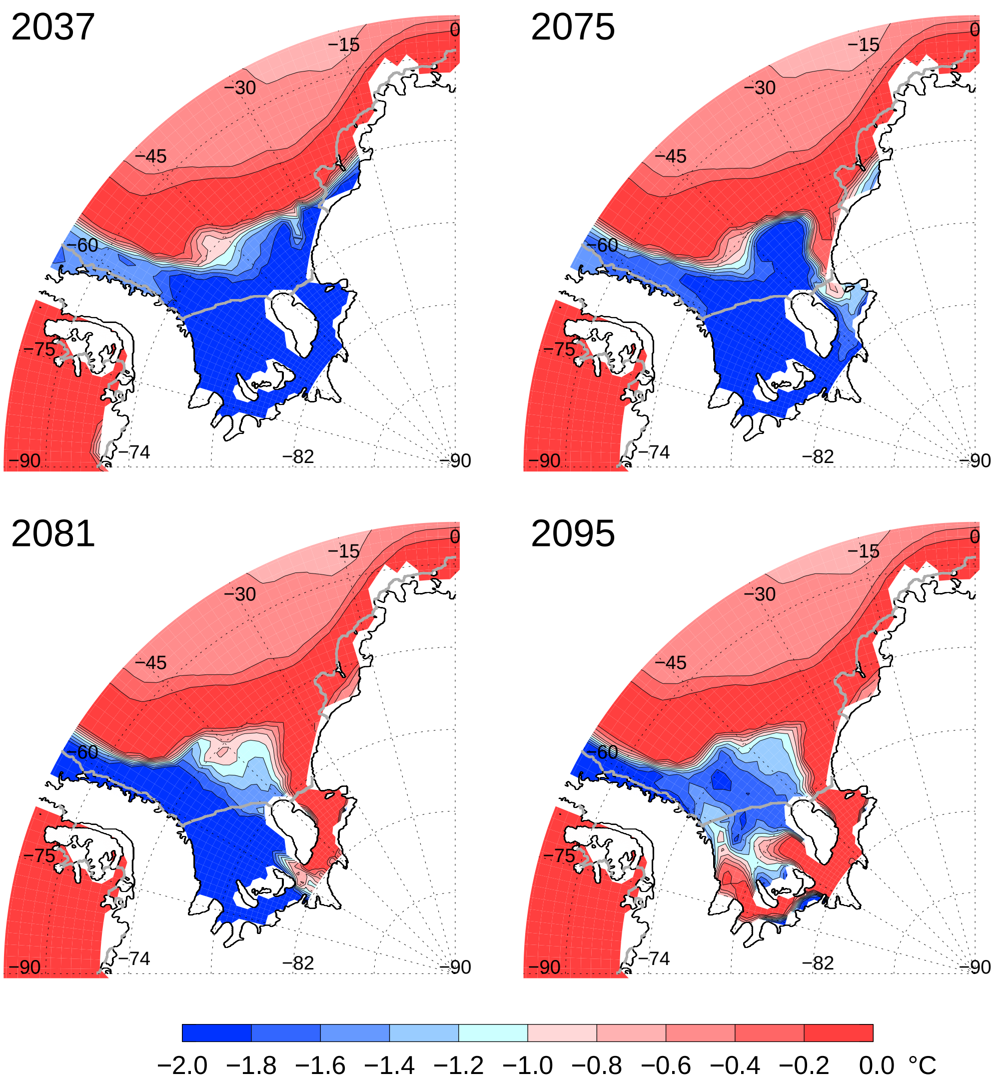
2037
2075
2081
2095
0
−15
−30
−45
−60
−75
−90
−74
−82
−90
−2.0 −1.8 −1.6 −1.4 −1.2 −1.0 −0.8 −0.6 −0.4 −0.2 0.0 °C

Figure 2: **Simulated evolution of near-bottom temperatures in the Weddell Sea.** Values are from 60 m above bottom for the period 2030-2099 of the HadCM3-B_A1B scenario. Warm pulses into the Filchner Trough (year 2037) are followed by a return of the shelf water masses to the cold state typical for today's conditions. The final (unrevoked) destruction of the slope front starts in 2066; by 2075 the tongue of slightly modified Warm Deep Water reaches the Filchner Ice Shelf front. It fills the deeper part of the Filchner Ice Shelf cavity and enters the Ronne cavity near the grounding line south of Berkner Island in 2081. By 2095, warm water fills most of the bottom layer of the Filchner cavity, reaching a quasi-steady state. Note that a trend in the water mass properties of the interior Weddell Sea is not associated with any of these processes.

261

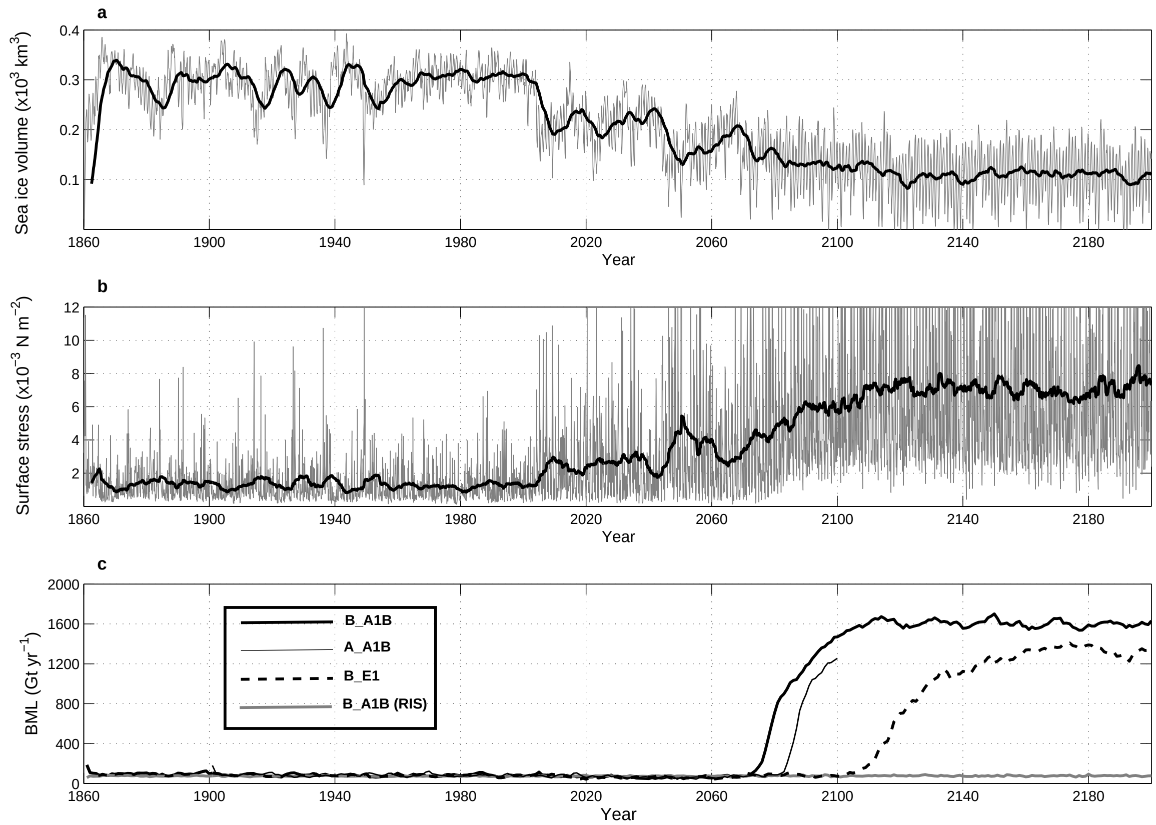
a
Sea ice volume (x10^3 km^3)
Year
b
Surface stress (x10^{-3} N m^{-2})
Year
c
BML (Gt yr^{-1})
B_A1B
A_A1B
B_E1
B_A1B (RIS)
Year

Figure 3: **Modelled timeseries (1860–2199) for the southeastern Weddell Sea.** **a**, area integrated (Fig. 1) sea ice volume for BRIOS forced with 20^{th}- century and A1B atmospheric output of the climate model HadCM3-B. Gray (black) lines represent monthly (5-year running) means. **b**, area mean ocean-surface stress, for same as **a**. Note that not only the long-term decrease of the sea-ice volume is reflected by an increase of the ocean-surface stress but that the coherence also holds for single events (e.g., around 1940 and 2050). A correlation coefficient is not provided because of the dominance of the long-term variability. **c**, basal mass losses (BML) in giga-tons per year (1 Gt = 10^{12} kg). Thin (thick) lines represent simulations forced with the atmospheric output of the climate models HadCM3-A (HadCM3-B). HadCM3-A forcing is available only for the period 1900–2099 and the A1B scenario (Tab. 1). Solid (dashed) lines represent results from forcing with 20^{th}- century and A1B (E1) output. Black lines show BML for the Filchner Ronne Ice Shelf and gray line for the Ross Ice Shelf (RIS). The inset provides a short definition of all lines.

Supplementary Information

In about year 2075 of our simulation warm water carried by the coastal current begins to enter continously the Filchner Trough (see Fig. 2; main text). To reveal the mechanism behind the redirection of the coastal current the atmospheric forcing of the HadCM3-B_A1B scenario was analyzed and additional experiments were performed.

A trend analysis for the period 2000–2099 of the atmospheric forcing (2-m temperature, specific humidity, short-wave/long-wave downward radiation, precipitation minus evaporation, and 10-m wind) indicates the largest linear trends for the 2-m temperature and the long-wave downward radiation. In the eastern Weddell Sea the trends for temperature and long-wave heat flux amount to 4 °C per century and 10 W m^{-2} per century, respectively. In addition, the analysis for the period 2000–2049 shows that about 80% of the changes occur in this time period. On top of the linear trends, strong year-to-year variability complicates the analysis of the mechanism controlling the redirection of the coastal current. Therefore, four additional experiments were conducted.

For the period 2000–2099 the linear trend was removed from all forcing variables and BRIOS was run with the new fields starting from year 2000 of the HadCM3-B_20^{th}-century experiment. HadCM3-B_detr shows no increase in mass loss at the Filchner-Ronne Ice Shelf (FRIS) base (Fig. S1; compare black and magenta lines).

For the period 2060–2069, prior to the onset of the redirection of the coastal current in the 'standard run' HadCM3-B_A1B, differences in sea-ice thickness, sea-ice concentration and ocean-surface stress (at the ice–ocean interface) between HadCM3-B_A1B and HadCM3-B_detr experiments were calculated (Fig. S2). Over the Filchner Trough the sea ice is thinner by up to 2 m, the sea-ice concentration is reduced by up to 30%, and the ocean-surface stress is stronger by about 4 mN m^{-2}. This corresponds to an increase of the ocean-surface stress of more than 100% (see also Fig. 3b; main text).

According to this analysis we propose the following mechanism driving the redirection of the coastal current: The increase in 2-m temperature and long-wave downward radiation reduces the sea-ice thickness and concentration in the southeastern Weddell Sea, making the ice more mobile. Consequently, the stress at the ocean surface, which directs to the southwest, increases. The Ekman spiral deflects the deeper ocean current to the left, allowing the coastal current to enter the Filchner Trough.

Three more experiments were designed to test this hypothesis. In the first experiment all forcing fields were detrended except the 2-m temperature (HadCM3-B_2mt). This experiment shows, same as HadCM3-B-detr, no increase in mass loss at the FRIS base (Fig. S1; green line). The second experiment with all forcing fields detrended except the long-wave downward radiation (HadCM3-B_lwdw) displays again no increase in basal melting beneath FRIS (Fig. S1; blue line). Only the third experiment with all forcing fields detrended except the 2-m temperature and the long-wave downward radiation (HadCM3-B_2mt-lwdw) reveals a basal mass loss which is almost identical to the FRIS basal mass loss in the 'standard run', but delayed by about 10 years (Fig. S1; red line).

The comparison of sea-ice thickness, sea ice concentration, and ocean-surface stress of the experiments HadCM3-B_2mt-lwdw and HadCM3-B_detr in the southern Weddell Sea for the period 2070-79 (Fig. S3) is very similar to the results shown in Fig. S2. This indicates that the trends in 2-m temperature and long-wave downward radiation explain virtually all of the reduction of sea-ice thickness and concentration, and the increase in ocean-surface stress over the Filchner Trough. The trends in the other forcing variables (e.g. wind) are not negligible but only contribute to a triggering of the redirection of the coastal current and, consequently, the increase in FRIS basal mass loss 10 years earlier. Essential for the change in the ocean-surface stress therefore is the thermodynamically forced reduction of sea-ice concentration and thickness over the southeastern Weddell Sea continental shelf (Fig. 1; main text).

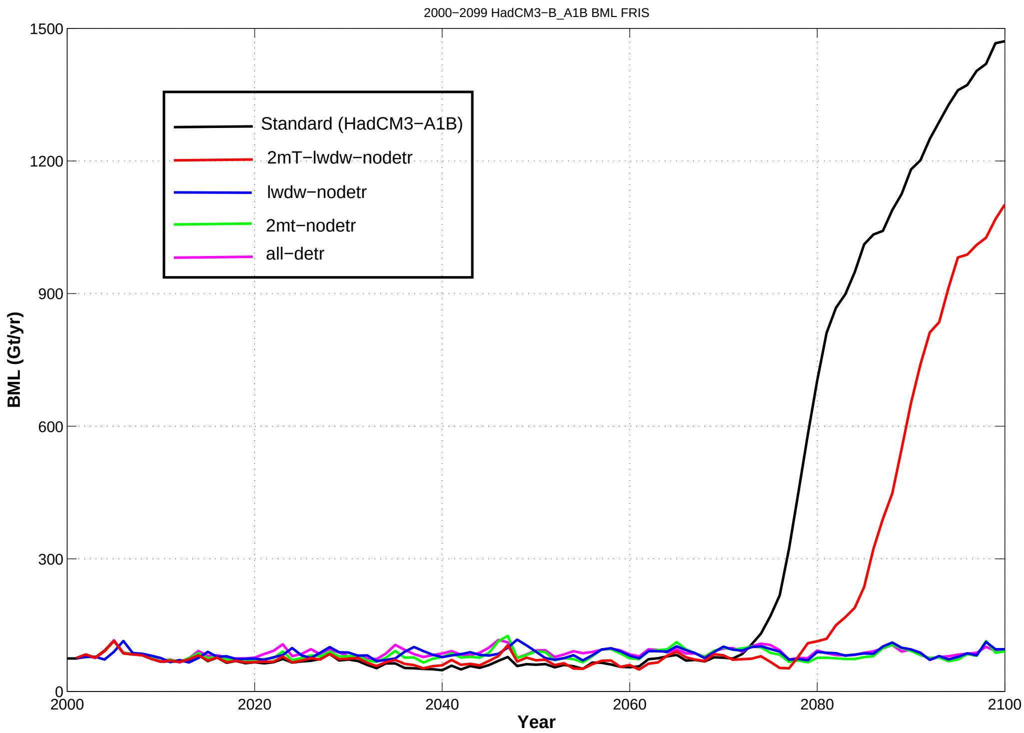

315 Figure S1: The 2000-2099 basal mass loss (Gt yr^{-1}) of the Filchner-Ronne Ice Shelf for HadCM3-B_A1B (black line), for the run with all forcing fields detrended (magenta), for all forcing fields detrended except the 2-m temperature (green), for all forcing fields detrended except the long-wave downward radiation (blue), and for all forcing fields detrended except the 2-m temperature plus the long-wave downward radiation (red).

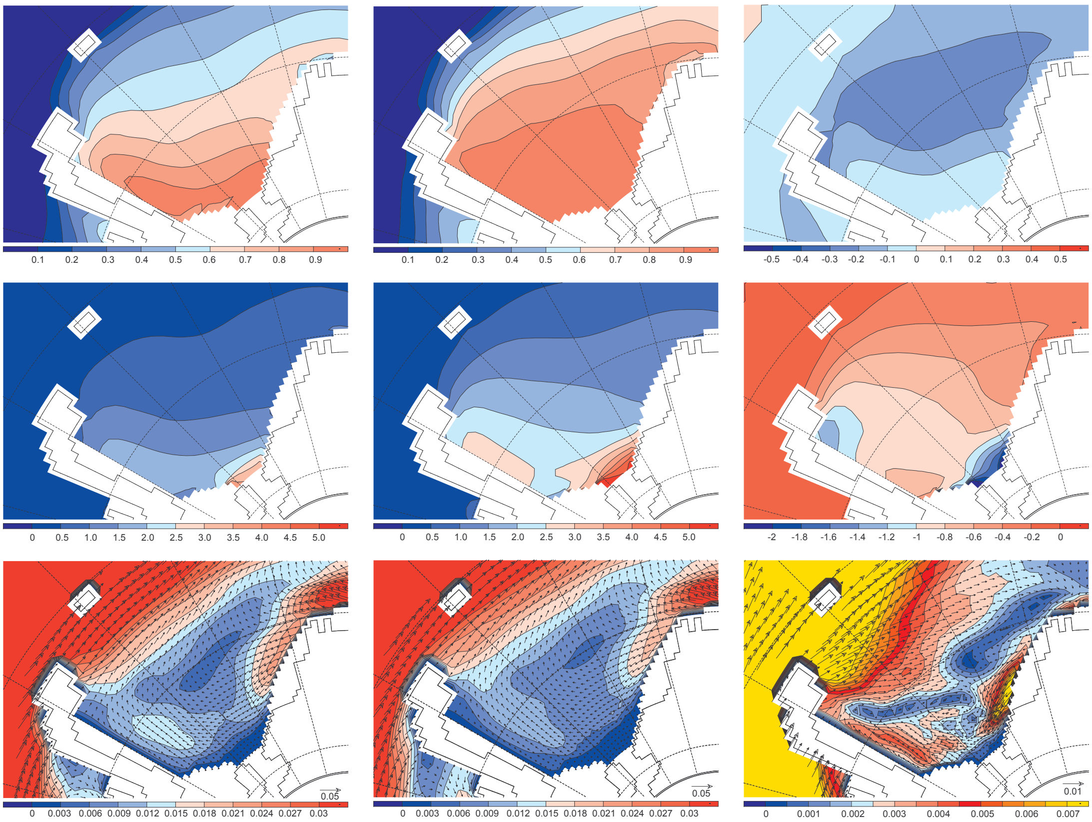

Figure S2: Mean sea-ice concentration (%) (upper row), sea-ice thickness (m) (middle row) and ocean-surface stress (N m^{-2}) (lower row) for the period 2060–2069 for the baseline experiment HadCM3-B_A1B (left column), the HadCM3-B_detr experiment (middle column), and for the difference between HadCM3-B_A1B and HadCM3-B_detr (right column).

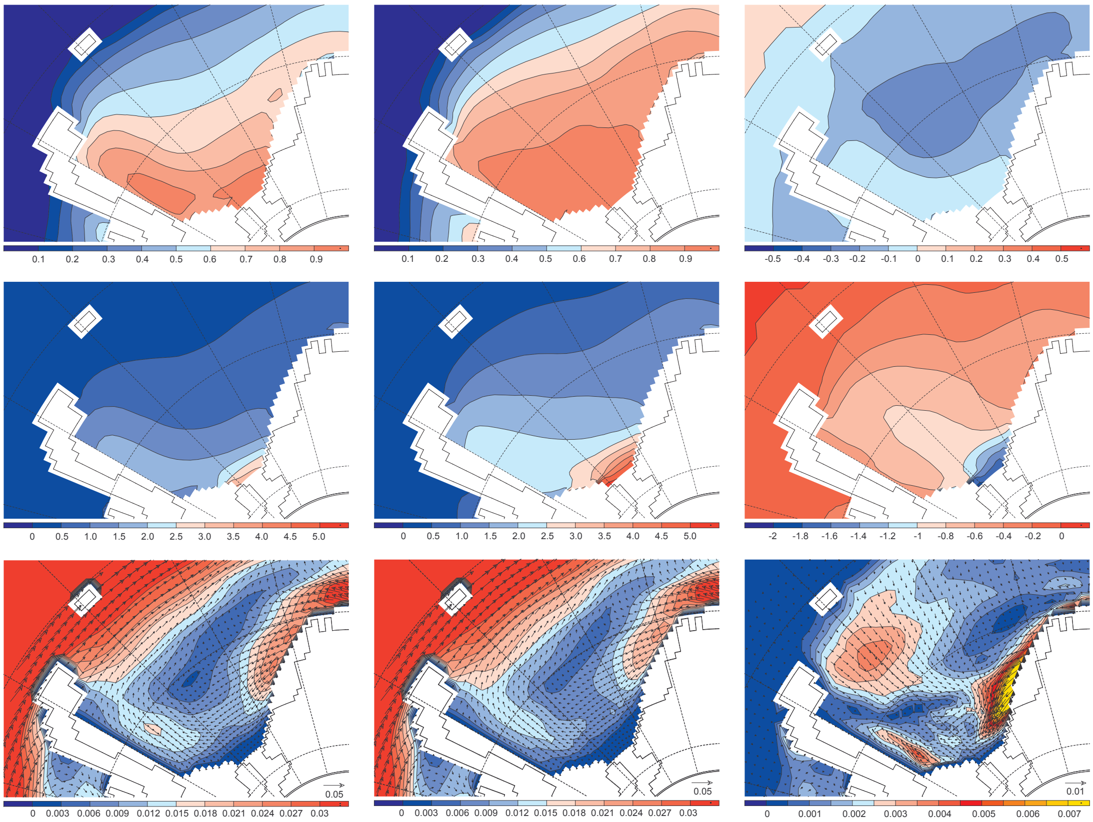

Figure S3: Mean sea-ice concentration (%) (upper row), sea-ice thickness (m) (middle row) and ocean-surface stress (N m^{-2}) (lower row) of the period 2070–2079 for the experiments HadCM3-B_2mt-lwdw (left column), HadCM3-B_detr (middle column), and for the difference between HadCM3-B_d2mt-lwdw and HadCM3-B_detr (right column).

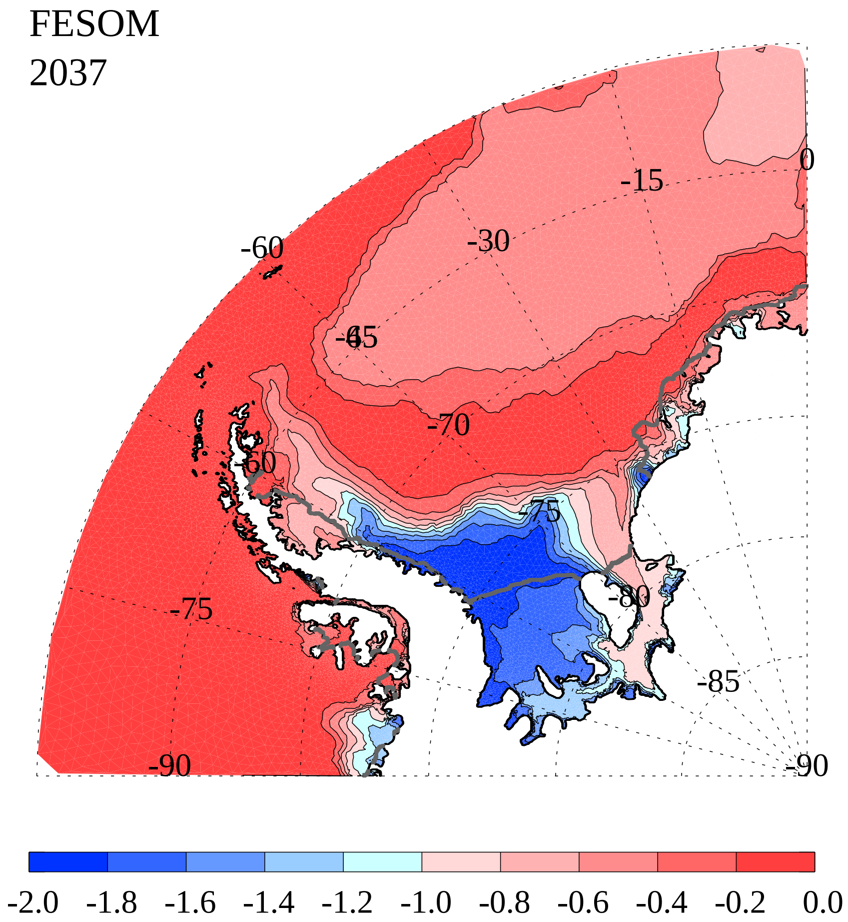

Figure S4: Distribution of near-bottom temperature (60 m above bottom) in the Weddell Sea for the year 2037 from FESOM using the HadCM3-B_A1B scenario. In contrast to the BRIOS results (Fig. 2: year 2037) early pulses of warm water into the Filchner Trough (Fig. 1) reach southern portions of the Filchner Ice Shelf cavity. Ice shelf fronts are marked by the thick gray line.

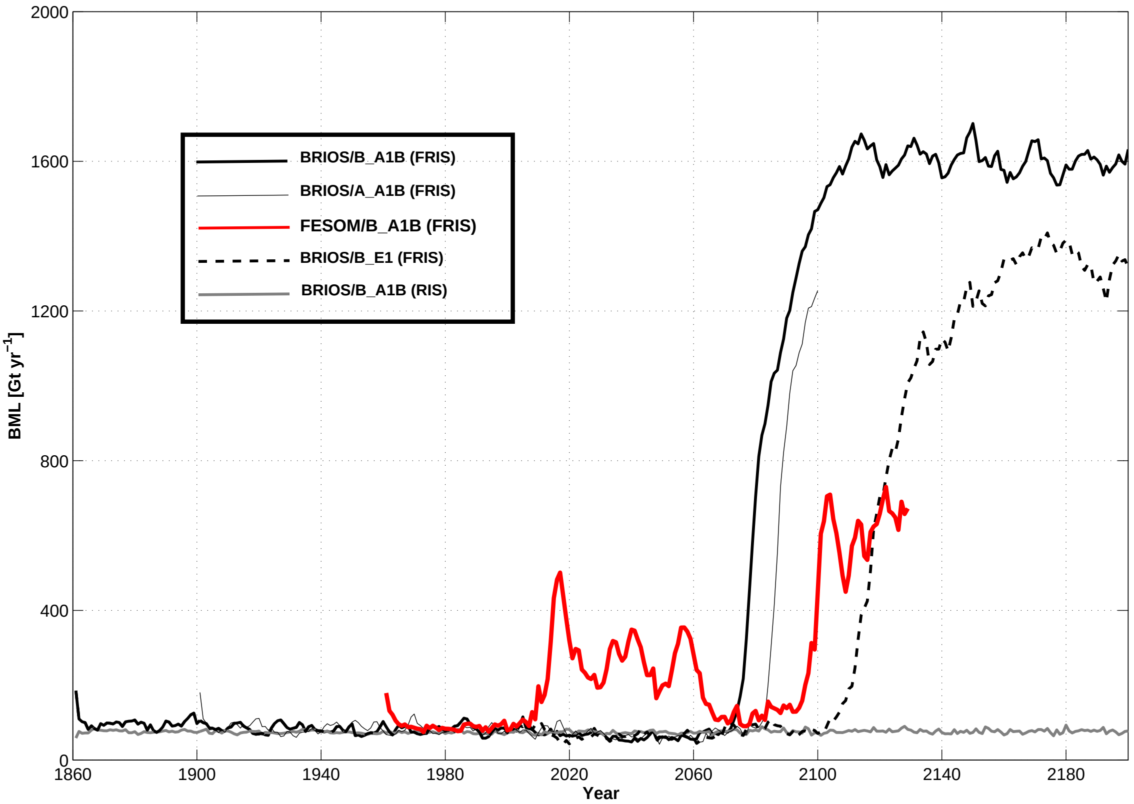

Figure S5: BRIOS basal mass losses in giga-tons per year (1 Gt = 10^{12} kg) for the Filchner Ronne Ice Shelf (black lines) and Ross Ice Shelf (gray line) using 20^{th} century, and A1B (solid lines) and E1 (dashed line) atmospheric forcing of the climate models HadCM3-A (thin line) and HadCM3-B (thick lines), complemented by the FESOM basal mass loss for the Filchner Ronne Ice Shelf (red line) using 20^{th} century and A1B atmospheric forcing of the climate model HadCM3-B (see insert).convert Due to computational constraints, which are imposed by the large number of grid nodes (1.85 million) and the small time-step (180 seconds), the FESOM time series starts in 1960 and has reached 2132 at the time of writing.